PHYSICAL REVIEW B **97**, 094418 (2018)

Biaxial stress driven tetragonal symmetry breaking and high-temperature ferromagnetic semiconductor from half-metallic CrO_2

Xiang-Bo Xiao and Bang-Gui Liu*
Beijing National Laboratory for Condensed Matter Physics, Institute of Physics, Chinese Academy of Sciences, Beijing 100190, China and School of Physical Sciences, University of Chinese Academy of Sciences, Beijing 100190, China

(Received 11 July 2017; revised manuscript received 23 December 2017; published 16 March 2018)

It is highly desirable to combine the full spin polarization of carriers with modern semiconductor technology for spintronic applications. For this purpose, one needs good crystalline ferromagnetic (or ferrimagnetic) semiconductors with high Curie temperatures. Rutile CrO_2 is a half-metallic spintronic material with Curie temperature 394 K and can have nearly full spin polarization at room temperature. Here, we find through first-principles investigation that when a biaxial compressive stress is applied on rutile CrO_2, the density of states at the Fermi level decreases with the in-plane compressive strain, there is a structural phase transition to an orthorhombic phase at the strain of −5.6%, and then appears an electronic phase transition to a semiconductor phase at −6.1%. Further analysis shows that this structural transition, accompanying the tetragonal symmetry breaking, is induced by the stress-driven distortion and rotation of the oxygen octahedron of Cr, and the half-metal-semiconductor transition originates from the enhancement of the crystal field splitting due to the structural change. Importantly, our systematic total-energy comparison indicates the ferromagnetic Curie temperature remains almost independent of the strain, near 400 K. This biaxial stress can be realized by applying biaxial pressure or growing the CrO_2 epitaxially on appropriate substrates. These results should be useful for realizing full (100%) spin polarization of controllable carriers as one uses in modern semiconductor technology.

DOI: 10.1103/PhysRevB.97.094418

I. INTRODUCTION

It is always of much interest to search for high-performance spintronic materials [1–4]. Full (100%) spin polarization can be realized in half-metallic materials [4,5] such as rutile CrO_2 [6,7,9,10], because one of the two spin channels is metallic and the other has a semiconductor gap. For rutile CrO_2, ferromagnetic Curie temperature can reach 394 K and great effort has been made to understand the physics in it and achieve high-quality materials for full spin polarization [8,11–18]. It is also interesting to seek half-metallic materials based on semiconductors [4,19–24]. Furthermore, one naturally hopes to combine the full polarization with modern semiconductor technology. For this purpose, one needs crystalline ferromagnetic (or ferrimagnetic) semiconductors with high Curie temperatures and then chooses appropriate dopants for controllable carriers. In this direction, many good materials have been found, and among them, perovskite Ca_2CrReO_6, Ca_2FeReO_6, and Sr_2CrOsO_6 are ferrimagnetic semiconductors with high Curie temperatures 360 K, 522 K, and 725 K, respectively [25–28]. Along this line, it is hopeful to realize full (or at least nearly full) spin polarization for controllable concentrations of high-mobility carriers beyond room temperature.

Here, we present strain-induced tetragonal symmetry breaking in rutile CrO_2 and a high-temperature ferromagnetic semiconductor phase from the half-metallic CrO_2 in terms of first-principles calculation. Biaxial compressive stress is applied to rutile CrO_2 to make the in-plane lattice constants (a, b) reduce by up to −8%, with the other lattice constant (c) determined by stress equilibrium. The stress can make the horizontal bonds (Cr-O and O-O) compress substantially and keep the side bond-angle (between two oblique bonds) decrease notably, but the oblique bonds (Cr-O) remain almost unchanged. With the stress increasing, the density of states (DOS) at the Fermi level decreases substantially, and finally the rutile CrO_2 becomes an orthorhombic phase when a is compressed by 5.6%. Keeping the biaxial stress increasing, there will be an electronic phase transition to the ferromagnetic semiconductor phase. It is very interesting that for all the compression ratios, the magnetic energies per formula unit remain almost unchanged and then the Curie transition temperature still remains near 400 K. Our analysis indicates that these phase transitions are driven by the distortion and rotation of the oxygen octahedron of Cr and the resulting crystal field splitting enhancement. This could open a door to achieve crystalline ferromagnetic semiconductors with high Curie temperatures. More detailed results will be presented in the following.

II. COMPUTATIONAL DETAILS

Our density-functional theory calculations are done with the Vienna package WIEN2K [29], which is a full-potential augmented plane wave plus local orbital program within the density-functional theory [30,31]. For total energy calculation of rutile and orthorhombic CrO_2, we take the generalized gradient approximation (GGA) [32] for the exchange-correlation potential. The scalar approximation is taken for the relativistic effects of valence states. For improving the electronic structure calculations, we use modified Becke-Johnson (mBJ) [33]

---

*bgliu@iphy.ac.cn

2469-9950/2018/97(9)/094418(7)

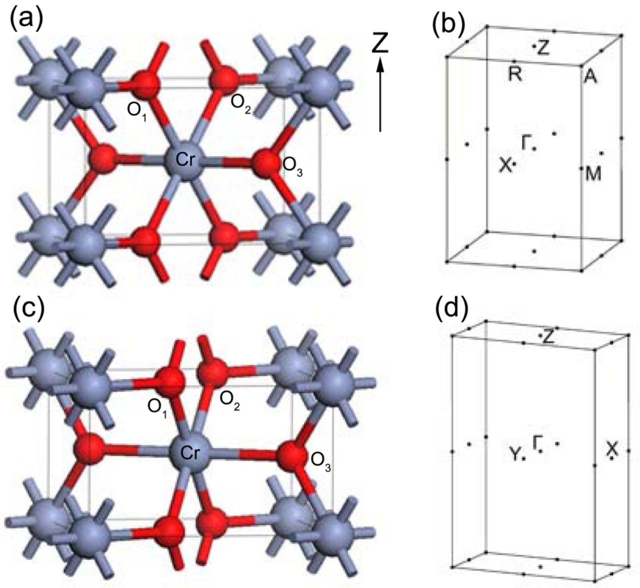

FIG. 1. The crystal structure (a) and the Brillouin zone (b) of rutile phase ($P4_2/mnm$), and the crystal structure (c) and the Brillouin zone (d) of the orthorhombic phase ($Pnnm$) of CrO_2.

TABLE I. Optimized structural parameters (a, b, c, u_x, and u_y), total energy per formula unit (E), and semiconductor gap (E_g) of CrO_2 for different in-plane lattice constant d and its relative change $\Delta d/d_0$ as defined in the text. The semiconductor gap (E_g) values are calculated with mBJ.

$\Delta d/d_0$(%)	a (Å)	b (Å)	c (Å)	(u_x,u_y)	E (eV)	E_g (eV)
0	4.451	-	2.932	(0.304,0.304)	0	-
−3.0	4.317	-	3.000	(0.305,0.305)	0.130	-
−5.0	4.228	-	3.046	(0.306,0.306)	0.386	-
−5.5	4.206	-	3.062	(0.306,0.306)	0.474	-
−5.8	4.214	4.172	3.061	(0.309,0.301)	0.530	-
−6.0	4.226	4.143	3.065	(0.314,0.297)	0.566	-
−6.5	4.234	4.091	3.075	(0.319,0.292)	0.676	0
−7.0	4.221	4.059	3.087	(0.322,0.290)	0.786	0.03
−8.0	4.216	3.977	3.109	(0.328,0.284)	1.044	0.05

exchange potential plus GGA correlation potential for the exchange-correlation potential. The muffin-tin radii (R_{mt}) of Cr and O atom are optimized to achieve high accuracy. We use 3000 k points in the Brillouin zone and set $R_{\mathrm{mt}} \times K_{\max}$ to 7.0, and in addition, we make angular momentum expansion up to $l_{\max} = 10$ in the muffin tins. When the integrated absolute value of the charge difference per formula unit, $\int |\rho_n - \rho_{n-1}| dr$, between the input charge density [$\rho_{n-1}(r)$] and the output charge density [$\rho_n(r)$] is less than $0.0001|e|$, where e is the electron charge, the self-consistent calculation will be considered to be converged. The spin-orbit coupling is also taken into account to investigate the spin polarization at the Fermi level.

III. RESULTS AND DISCUSSION

A. Strain-dependent structure parameters

Rutile CrO_2 assumes a tetrahedral structure with the space group $P4_2/mnm$ (#136) [6,7,9,10], as shown in Fig. 1. There are two formula units in the unit cell. Two chromium atoms are located at (0,0,0) and $(\frac{1}{2},\frac{1}{2},\frac{1}{2})$ in the internal coordinates, and four oxygen atoms at $(u,u,0)$, $(1\text{-}u,1\text{-}u,0)$, $(\frac{1}{2}+u,\frac{1}{2}\text{-}u,\frac{1}{2})$, and $(\frac{1}{2}\text{-}u,\frac{1}{2}+u,\frac{1}{2})$, respectively, where u ($\leqslant 1$) is a dimensionless internal coordinate parameter. We have fully optimized the lattice constants (a and c) and the internal coordinate parameter u by using GGA. The resulting equilibrium structural parameters (a_0, c_0, and u_0) are equivalent to 4.4507 Å, 2.9317 Å, and 0.304, respectively. The electronic structure is half metallic, which is consistent with previous DFT-calculated results and experimental observations [6,7,9,10].

Because large uniaxial stress can make the rutile phase transit to an orthorhombic phase ($Pnnm$, No. 58), we also plot its crystal structure and corresponding Brillouin zone in Fig. 1. For this structure under uniaxial stress, we have three lattice constants (a, b, and c) and two internal coordinate parameters (u_x,u_y). Because the stress is always uniaxial, it is convenient to describe the in-plane strain in a unified way. For this purpose, we introduce a parameter d to equal a for the rutile phase and $\sqrt{ab}$ for the orthorhombic phase, and then use $\Delta d/d_0 = (d - d_0)/d_0$, with $d_0 = a_0$, to express the in-plane strain.

To manipulate the electronic structure, we can apply a biaxial stress to the rutile CrO_2. Such stress can be realized by applying pressure along the x and y axes or growing the rutile CrO_2 as epitaxial [001] thin films on some suitable substrates. Since tensile stress has limited effect on the electronic states of the CrO_2 near the Fermi level, we will concentrate on compressive stress within the x-y plane. It is clear that $\Delta d/d_0 = \Delta a/a_0 = 0$ corresponds to the equilibrium lattice. For the rutile phase, with a given in-plane lattice constant $a < a_0$, we make a full structural optimization to determine the other lattice constant c and the internal parameter u. For the orthorhombic phase, with $d = \sqrt{ab}$ used to correspond the a parameter in the rutile phase, we also make full optimization to determine the five parameters: a, b, c, u_x, and u_y. The total energy of the strained CrO_2 is calculated with the optimized strained crystal structure. We have done a series of optimization with $0 > \Delta d/d_0 \geqslant -8\%$. The structural parameters (a, b, c, u_x, and u_y) and total energy (E) values are summarized in Table I.

At first, we assume that CrO_2 is in the rutile phase. As the in-plane compressive strain ($-\Delta d/d_0$) increases ($d = a$ decreases), c increases, and the internal parameter u increases slightly. The opposite trend of a and c reflects the trend that, with stress applied, the volume tries to remain unchanged. Because c becomes large with the biaxial compression increasing, there is actually a tensile strain in the z axis. The stronger the compression is, the larger the energy E becomes, which is expected because the strain drives the CrO_2 to deviate from the equilibrium structure. When the in-plane strain reaches −5.6%, the rutile phase will transit to the orthorhombic phase, keeping the half-metallic feature. More importantly, there is a phase transition from the half-metallic phase to a semiconductor when the compression ratio of d reaches −6.1%. We visualize these trends of a, b, c, $u = (u_x,u_y)$ in Fig. 2(a) by plotting them as functions of the compression ratio, $\Delta d/d_0$. It is clear that the lattice constants change

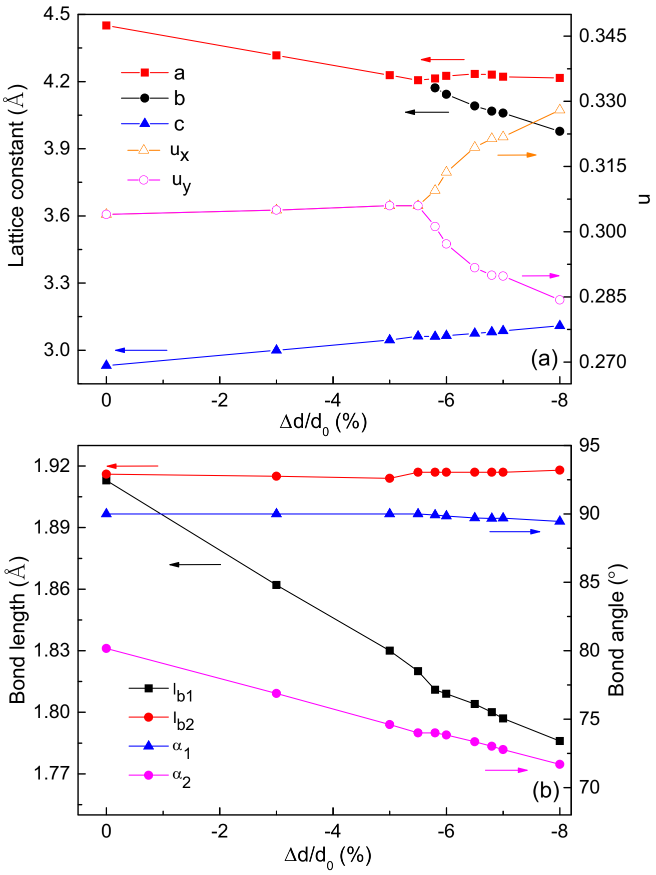

FIG. 2. The $\Delta d/d_0$ dependence of the structural parameters (a, b, c, u_x, u_y) (a) and the bond parameters ($l_{b1}, l_{b2}, \alpha_1, \alpha_2$) (b). The in-plane lattice constants and u parameters are different along the x and y axes in the orthorhombic phase, and the structural phase transition can also be seen in the curves of bond lengths and angles.

almost linearly with $\Delta d/d_0$ decreasing, and the parameter u has little change until $\Delta d/d_0$ reaches to the structural phase transition point. Entering the orthorhombic phase, both $a - b$ and $u_x - u_y$ increase notably.

It is vital to check the stability of ferromagnetic order and Curie temperature against the biaxial compression. Because the biaxial compression enhances the ferromagnetic exchange in the x-y plane and maybe weakens the ferromagnetic exchange in the z direction, we have constructed antiferromagnetic order along the z direction and compared their total energies with the ferromagnetic rutile or orthorhombic CrO_2 for $\Delta d/d_0 = 0, -3.0, -5.0, -6.0, -7.0, -8.0\%$, respectively. For the $\Delta d/d_0$ values, our calculated results show that the ferromagnetic CrO_2 is lower than the antiferromagnetic configuration by 0.320, 0.346, 0.352, 0.369, 0.373, and 0.378 eV per formula unit, respectively. Therefore, the ferromagnetic order is stable against spin fluctuation, and when the biaxial compression is applied, the Curie temperature should remain approximately the same as that of the equilibrium structure [4,16–18].

To find out the relationship between the electronic properties and the crystal structure, we also present in Table II the bond angles (α_1 and α_2) and the bond lengths (l_{b1} and l_{b2}) of CrO_2 for different $\Delta d/d_0$ values. Here, α_1 and α_2 denote the O1-Cr-O3 and O1-Cr-O2 bond angles, and l_{b1} and l_{b2} indicate the lengths of the Cr-O3 and Cr-O2 bonds, respectively. It should be noted that the Cr-O3 bond is always perpendicular to the Cr-O1 and Cr-O2 bonds for the rutile phase, and the angle deviates from 90° for the orthorhombic phase. We plot in Fig. 2(b) the bond lengths and the bond angles as functions of different compression ratios of lattice constant, $\Delta d/d_0$. It is clear that the bond angle α_2 and the bond length l_{b1} almost linearly decrease with $\Delta d/d_0$ changing from 0 to −8%, whereas the other bond angle α_1 and bond length l_{b2} change only a little. Our analysis shows that the almost-linear decrease of the Cr-O3 bond length is caused directly by the decrease of the lattice constant d, and the Cr-O2 bond length remains almost unchanged because the decrease of the bond angle α_2 compensates the opposite changes of d and c.

TABLE II. The bond angles (α_1 and α_2) and bond lengths (l_{b1} and l_{b2}) for different $\Delta d/d_0$ values.

$\Delta d/d_0$ (%)	α_2 (°)	α_1 (°)	l_{b1}(Å)	l_{b2}(Å)
0	80.17	90.00	1.913	1.916
−3.0	76.88	90.00	1.862	1.915
−5.0	74.60	90.00	1.830	1.914
−5.5	74.00	90.00	1.820	1.917
−5.8	73.98	89.92	1.811	1.917
−6.0	73.84	89.85	1.809	1.917
−6.5	73.35	89.71	1.804	1.917
−7.0	72.77	89.69	1.797	1.917
−8.0	71.70	89.45	1.786	1.918

B. Electronic structures and phase transition

We present in Fig. 3 the total and partial DOS calculated with mBJ for three $\Delta d/d_0$ values: 0, −6.0%, and −8.0%. For the equilibrium structure [(Fig. 3(a)], we found through our mBJ calculations that there is a big gap in the minority spin channel around the Fermi level, but the band structure is metallic in the majority spin channel, which is consistent with the fact that rutile CrO_2 is half metallic [6,7,9,10]. As we decrease the lattice parameter d (or a), the total DOS at the Fermi level reduces in the majority spin channel, and we will meet the structural phase transition point and then obtain the orthorhombic phase. Figure 3(b) shows the DOS for $\Delta d/d_0 = -6.0\%$. When the lattice parameter d is compressed by more than 6.1%, it can be seen that the total DOS at the Fermi level becomes zero, as shown in Fig. 3(c) for $\Delta d/d_0 = -8.0\%$, and consequently we obtain a ferromagnetic semiconductor phase. These electronic structures show an electronic phase transition from half metal of rutile CrO_2 to ferromagentic semiconductor of the orthorhombic CrO_2 material. The low DOS near the Fermi level reflects that the O p electrons are distributed mainly out of the O muffin tin, which is consistent with the large DOS contribution from the interstitial region.

To investigate the electronic properties of these systems in detail, we have also calculated the orbit-resolved DOS. The detailed orbit-resolved density of states in the vicinity of the Fermi level for $\Delta d/d_0$ =0, −5.0%, −6.0%, and −8% are shown in Fig. 4. Here, we use the usual local coordinates and orbital convention for rutile and orthorhombic structures

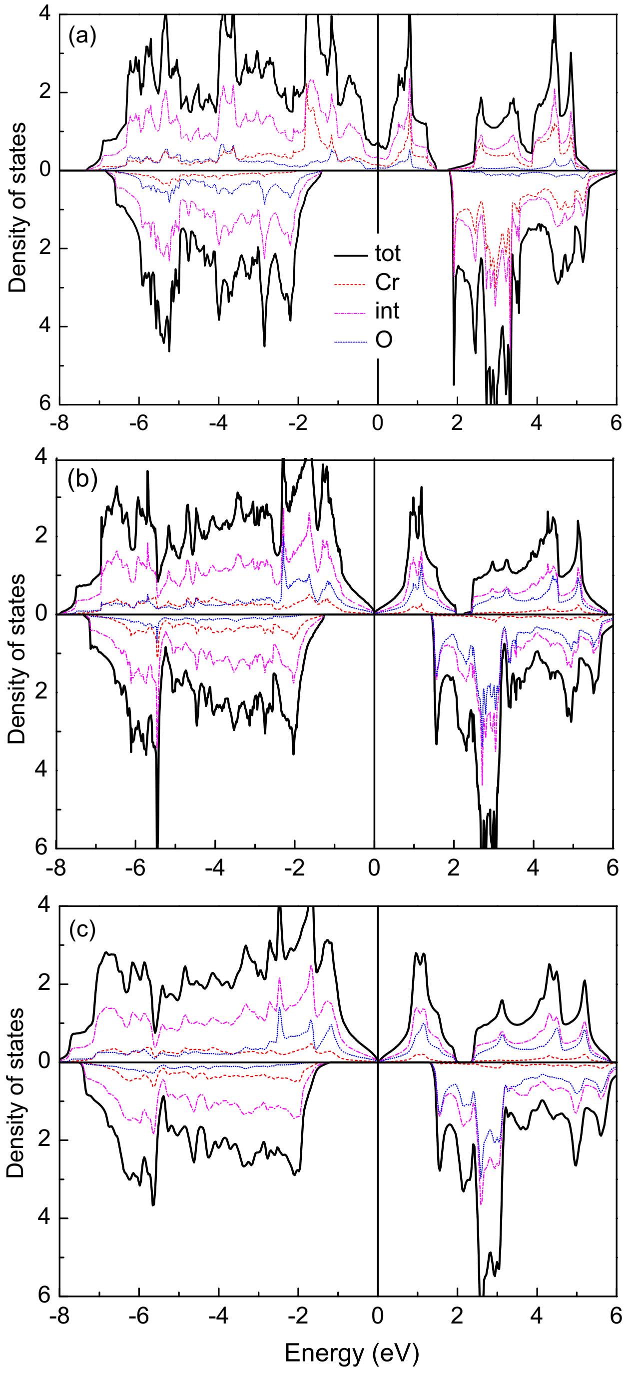

FIG. 3. Spin-resolved total and partial density of states of CrO_2 for (a) the rutile equilibrium structure, (b) the orthorhombic structure with d compressed by 6%, and (c) the orthorhombic structure with d compressed by 8%.

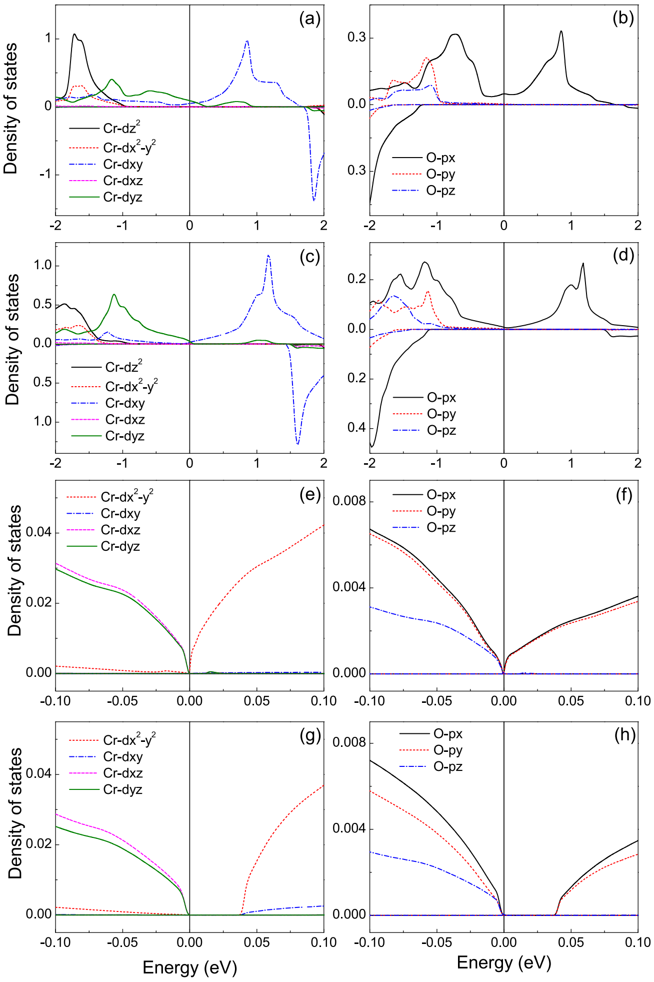

FIG. 4. Orbital-resolved partial density of states of Cr-d and O-p (a), (b) for the rutile equilibrium structure, (c), (d) for the rutile phase with d compressed by 5%, (e), (f) for the orthorhombic structure with d compressed by 6%, and (g), (h) for the orthorhombic structure with d compressed by 8%.

[8,11]. For the equilibrium structure, the Cr 3d states near the Fermi level consist of Cr d_{xy} and d_{yz} in the majority spin channel, as shown in Fig. 4(a). As for the O 2p states, the p_x orbital is dominant near the Fermi level, as shown in Fig. 4(b). As the lattice parameter d decreases, the main weights of the Cr d_{xy} and d_{yz} and O 2p orbitals gradually move away from the Fermi level and the DOS there becomes smaller and smaller. The results for $\Delta d/d_0 = -5.0\%$ are presented in Figs. 4(c) and 4(d). At $\Delta d/d_0 = -6.0\%$, as shown in Figs. 4(e) and 4(f), the DOS at the Fermi level is nearly zero, and the orbitals there are $d_{x^2-y^2}$, d_{xz}, d_{yz}, and the three p orbitals. At $\Delta d/d_0 = -6.1\%$, there is a gap open at the Fermi level, and the gap grows when the d is compressed further, reaching to 0.05 eV at $\Delta d/d_0 = -8.0\%$, as shown in Figs. 4(g) and 4(h). These imply that when $\Delta d/d_0$ is beyond -6.1%, the valence band top is occupied mainly by Cr d_{xz} and d_{yz} orbitals, and the conduction band bottom mainly by Cr $d_{x^2-y^2}$.

We present in Fig. 5 the band structures of strained CrO_2 for $\Delta d/d_0$ =0, -5.0%, -6.0%, and -8%. It is clear that without any strain, the rutile CrO_2 is a typical half-metal with a large gap in the minority-spin channel, as shown in Figs. 5(a) and 5(b). As we decrease the lattice parameter d, the bands near the Fermi level tend to move away from the Fermi level in the majority-spin channel, with the gap still remaining wide in the minority-spin channel. The majority-spin gap is approximately at the middle of the minority-spin gap. With $\Delta d/d_0 = -5\% \sim -6\%$, the conduction band minimum is at the Γ point in the Brillouin zone, and the valence band maximum at the Z point,

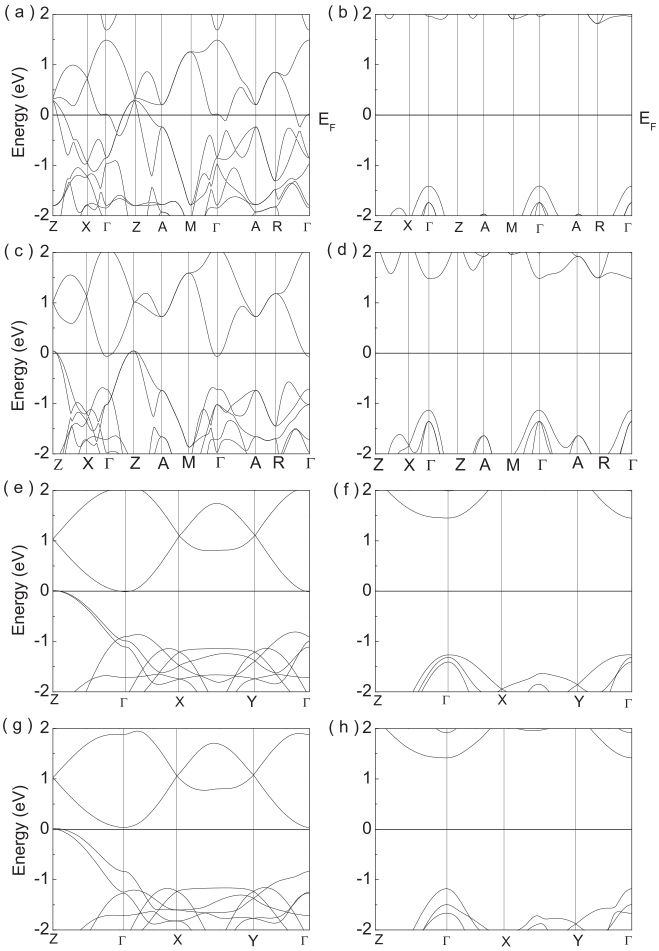

FIG. 5. Spin-polarized band structures of CrO_2 (a), (b) for the rutile equilibrium structure, (c), (d) for the rutile phase with d compressed by 5%, (e), (f) for the orthorhombic structure with d compressed by 6%, and (g), (h) for the orthorhombic structure with d compressed by 8%. The left column presents the majority-spin band structure, and the right column the minority-spin one.

which implies that the strained CrO_2 is a semimetal, as shown in Figs. 5(c)– 5(f). The transition happens at $\Delta d/d_0 = -6.1\%$, from which there is a narrow gap open at the Fermi level in the majority-spin channel, and then the strained CrO_2 is a semiconductor with an indirect gap. Combining with the DOS near the Fermi level, we can conclude that for $\Delta d/d_0 = -8\%$, the valence band maximum at the Z point consists mainly of d_{xz} and d_{yz}, or d_{yz-xz} in terms of another orbital convention [8,11], and the conduction band minimum at the Γ point mainly of $d_{x^2-y^2}$ orbital.

C. Further discussions

Furthermore, we show the strain dependence of the oxygen octahedron and the key bond lengths and bond angles in rutile and orthorhombic CrO_2 phases. In Fig. 6, we present the strain dependence of the bond length (l_{b1}) between Cr1 and O3 and the O-O bond length (l_O) that can be defined as the distance between O1 and O2. We can see in Fig. 2 and Table II that when the biaxial compressive stress is applied, both l_{b1} and α_2 decrease nearly linearly, but l_{b2} and α_1 remain nearly unchanged. The O-O bond length l_O also decreases with the compressive stress increasing. It is clear that the O-O bond length l_O is compressed more easily than the horizontal bond length l_{b1}. This implies that it is more easy to compress the bond angle α_2 than to compress the horizontal length l_{b2}. These changes of the bond lengths and angles mean that the oxygen octahedron is distorted and there is a small rotation around the z axis.

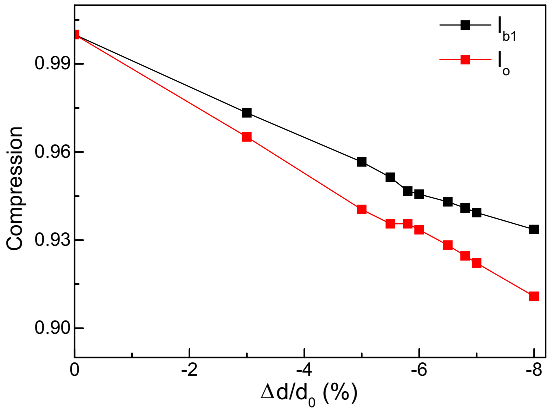

FIG. 6. The strain-dependent compression ratios of the horizontal bond (l_{b1}) and the O-O distance (l_O).

We present in Fig. 7 the elastic energy and stress as functions of the in-plane compressive ratio $\Delta d/d_0$. With $|\Delta d/d_0| \geqslant 5.6\%$, the rutile CrO_2 transits to the orthorhombic phase that features smaller energy and smaller stress for the same $|\Delta d/d_0|$. The stress can be realized by applying biaxial pressure, or growing the CrO_2 on substrates with smaller in-plane lattice constants. We can realize such compression by growing the CrO_2 on good oxide substrates such as CoO, MgO, NiO, and $BaSnO_3$ [34,35]. For these four substrates, the lattice mismatch is between −3.4% and −7%, and the stress is between 11.5 and 23.8 GPa. Accordingly, the first three heterostructures (CrO_2/CoO, CrO_2/MgO, CrO_2/NiO) should still be half-metallic, and the heterostructure $CrO_2/BaSnO_3$ should be semiconducting. It is interesting that EuO epitaxial thin films have been grown on $SrTiO_3$ [36], Si [37], and MgO [38,39]. Actually, a giant compressive strain of −22% (due to lattice mismatch of $|a_{EuO}/a_{MgO} - 1| = 22\%$) has been realized in high-quality crystalline epitaxial EuO/MgO(001) systems [38,39]. An atomically sharp, crystalline EuO/MgO(001) transport surface is established thanks to the fully relaxed oxide heteroepitaxy [38,39]. Because of the similarity to the EuO/MgO(001) oxide epitaxial system, it is believed that CrO_2 as an oxide, even with the large strain, can be epitaxially grown on some oxide substrates, such as CoO, MgO, NiO, and $BaSnO_3$. Therefore, these strained CrO_2 thin films should be experimentally realizable on some appropriate substrates. Because the Curie temperature for such strain values should remain almost the same as that of equilibrium strain-free CrO_2, we can manipulate the transport properties of the CrO_2 at room temperature by growing it on appropriate substrates.

As for the electron correlation in rutile CrO_2, it has been proved to be weak by the latest bulk-sensitive soft-X-ray ARPES [40], in contrast to previous experimental results [4]. Because of metastability, the surface of CrO_2 material instantly

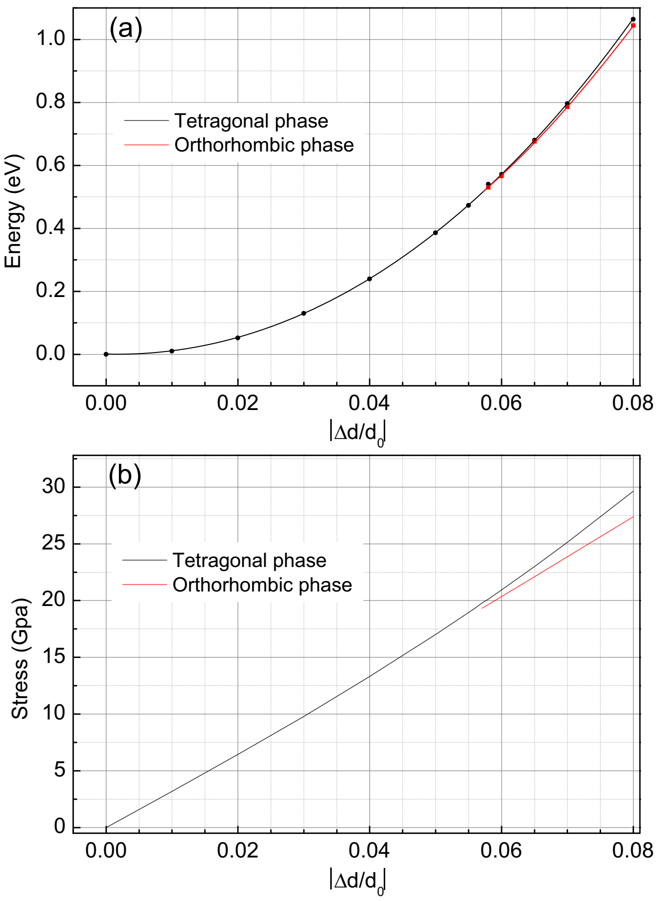

FIG. 7. The $|\Delta d/d_0|$ dependence of total energy (a) and stress (b). It can be seen that for $|\Delta d/d_0| \geqslant 5.6\%$, the total energy of the orthorhombic phase is only a little smaller than that of the tetragonal phase, but the stress is much smaller.

reduces to amorphous Cr_2O_3. Successful direct access to the native bulk electronic structure of CrO_2 is achieved because this method allows for penetrating through the Cr_2O_3 surface layer and measuring the intrinsic electronic dispersions and Fermi surface of CrO_2 samples [40]. Therefore, our DFT computational approach is reasonable and the calculated results are reliable, which is supported by the bulk-sensitive experiment.

IV. CONCLUSION

We have investigated the structural, magnetic, electronic properties of the rutile and orthorhombic CrO_2 phases under biaxial compressive stress through first-principles calculation. mBJ exchange potential is used to improve the description of the electronic structure. The biaxial compressive stress makes the in-plane lattice parameter $d = a$ (or $d = \sqrt{ab}$) decrease and the out-of-plane c increase. Correspondingly, the two horizontal Cr-O and O-O bond lengths and the side O-Cr-O bond-angle decrease linearly, but the oblique bond lengths remain almost unchanged. There is a structural phase transition at $\Delta d/d_0 = -5.6\%$. Our total energy comparison shows that the Curie temperature of the strained CrO_2 remains almost the same as that (near 400 K) without any stress. As for the electronic structure, the DOS near the Fermi level decreases with the d becoming small and there is a half-metal-semiconductor transition at $\Delta d/d_0 = -6.1\%$. Full spin polarization can be realized for controllable concentration of carriers by usual gating or doping used in modern semiconductor technology. Our further analysis shows that this semiconducting ferromagnetic phase is driven by the biaxial-stress-induced distortion of the oxygen octahedron of Cr in the crystal structure. This biaxial compression can be realized by applying biaxial pressure or growing CrO_2 epitaxially on appropriate substrates. Therefore, these could pave a road to achieve good ferromagnetic semiconductors for spintronic applications.

ACKNOWLEDGMENTS

This paper is supported by the Nature Science Foundation of China (Grant No. 11574366), by the Strategic Priority Research Program of the Chinese Academy of Sciences (Grant No. XDB07000000), and by the Department of Science and Technology of China (Grant No. 2016YFA0300701). All the numerical calculations were performed in the Milky Way #2 Supercomputer system at the National Supercomputer Center of Guangzhou, Guangzhou, China.

---

[1] S. A. Wolf, D. D. Awschalom, R. A. Buhrman, J. M. Daughton, S. von Molnar, M. L. Roukes, A. Y. Chtchelkanova, and D. M. Treger, Science **294**, 1488 (2001).
[2] W. E. Pickett and J. S. Moodera, Phys. Today **54**(5), 39 (2001).
[3] F. J. Jedema, A. T. Filip, and B. van Wees, Nature **410**, 345 (2001).
[4] M. I. Katsnelson, V. Y. Irkhin, L. Chioncel, A. I. Lichtenstein, and R. A. de Groot, Rev. Mod. Phys. **80**, 315 (2008).
[5] R. A. de Groot, F. M. Mueller, P. G. van Engen, and K. H. J. Buschow, Phys. Rev. Lett. **50**, 2024 (1983).
[6] K. Schwarz, J. Phys. F **16**, L211 (1986).
[7] K. P. Kamper, W. Schmitt, G. Guntherodt, R. J. Gambino, and R. Ruf, Phys. Rev. Lett. **59**, 2788 (1987).
[8] M. A. Korotin, V. I. Anisimov, D. I. Khomskii, and G. A. Sawatzky, Phys. Rev. Lett. **80**, 4305 (1998).
[9] Y. S. Dedkov, M. Fonine, C. Konig, U. Rudiger, G. Guntherodt, S. Senz, and D. Hesse, Appl. Phys. Lett. **80**, 4181 (2002).
[10] J. Kunes, P. Novak, P. M. Oppeneer, C. Konig, M. Fraune, U. Rudiger, G. Guntherodt, and C. Ambrosch-Draxl, Phys. Rev. B **65**, 165105 (2002).
[11] A. Toropova, G. Kotliar, S. Y. Savrasov, and V. S. Oudovenko, Phys. Rev. B **71**, 172403 (2005).
[12] R. S. Keizer, S. T. B. Goennenwein, T. M. Klapwijk, G. Miao, G. Xiao, and A. Gupta, Nature **439**, 825 (2006).
[13] G. M. Muller, J. Walowski, M. Djordjevic, G.-X. Miao, A.

Gupta, A. V. Ramos, K. Gehrke, V. Moshnyaga, K. Samwer, J. Schmalhorst *et al.*, Nat. Mater. **8**, 56 (2009).

[14] M. S. Anwar, F. Czeschka, M. Hesselberth, M. Porcu, and J. Aarts, Phys. Rev. B **82**, 100501(R) (2010).

[15] M. S. Anwar and J. Aarts, Phys. Rev. B **88**, 085123 (2013).

[16] H. Fujiwara, M. Sunagawa, K. Terashima, T. Kittaka, T. Wakita, Y. Muraoka, and T. Yokoya, Appl. Phys. Lett. **106**, 202404 (2015).

[17] H. Takeda, Y. Shimizu, Y. Kobayashi, M. Itoh, T. Jin-no, M. Isobe, Y. Ueda, S. Yoshida, Y. Muraoka, and T. Yokoya, Phys. Rev. B **93**, 235129 (2016).

[18] A. Singh, C. Jansen, K. Lahabi, and J. Aarts, Phys. Rev. X **6**, 041012 (2016).

[19] S. Sanvito and N. A. Hill, Phys. Rev. B **62**, 15553 (2000).

[20] H. Akinaga, T. Manago, and M. Shirai, Jpn. J. Appl. Phys. **39**, L1118 (2000).

[21] I. Galanakis, Phys. Rev. B **66**, 012406 (2002).

[22] B.-G. Liu, Phys. Rev. B **67**, 172411 (2003).

[23] W. H. Xie, Y. Q. Xu, B. G. Liu, and D. G. Pettifor, Phys. Rev. Lett. **91**, 037204 (2003).

[24] S.-D. Li and B.-G. Liu, Appl. Phys. Lett. **104**, 122408 (2014).

[25] H. Kato, T. Okuda, Y. Okimoto, Y. Tomioka, K. Oikawa, T. Kamiyama, and Y. Tokura, Phys. Rev. B **69**, 184412 (2004).

[26] Y. Krockenberger, K. Mogare, M. Reehuis, M. Tovar, M. Jansen, G. Vaitheeswaran, V. Kanchana, F. Bultmark, A. Delin, F. Wilhelm, A. Rogalev, A. Winkler, and L. Alff, Phys. Rev. B **75**, 020404(R) (2007).

[27] O. N. Meetei, O. Erten, M. Randeria, N. Trivedi, and P. Woodward, Phys. Rev. Lett. **110**, 087203 (2013).

[28] S. Gong, S.-D. Guo, P. Chen, and B.-G. Liu, RSC Adv. **5**, 63165 (2015).

[29] P. Blaha, K. Schwarz, P. Sorantin, and S. B. Trickey, Comput. Phys. Commun. **59**, 399 (1990).

[30] P. Hohenberg and W. Kohn, Phys. Rev. **136**, B864 (1964).

[31] W. Kohn and L. J. Sham, Phys. Rev. **140**, A1133 (1965).

[32] J. P. Perdew, K. Burke, and M. Ernzerhof, Phys. Rev. Lett. **77**, 3865 (1996).

[33] F. Tran and P. Blaha, Phys. Rev. Lett. **102**, 226401 (2009).

[34] D. R. Lide, *Handbook of Chemistry and Physics*, 79th ed., (CRC, Boca Raton, FL, 1998).

[35] Y. Hinatsu, J. Solid State Chem. **122**, 384 (1996).

[36] P. Lomker, T. C. Rodel, T. Gerber, F. Fortuna, E. Frantzeskakis, P. L. Fevre, F. Bertran, M. Muller, and A. F. Santander-Syro, Phys. Rev. Mater. **1**, 062001(R) (2017).

[37] L. L. Lev, D. V. Averyanov, A. M. Tokmachev, F. Bisti, V. A. Rogalev, V. N. Strocov, and V. G. Storchak, J. Mater. Chem. C **5**, 192 (2017).

[38] C. Caspers, A. Gloskovskij, W. Drube, C. M. Schneider, and M. Muller, Phys. Rev. B **88**, 245302 (2013).

[39] G. M. Prinz, T. Gerber, A. Lorke, and M. Muller, Appl. Phys. Lett. **109**, 202401 (2016).

[40] F. Bisti, V. A. Rogalev, M. Karolak, S. Paul, A. Gupta, T. Schmitt, G. Guntherodt, V. Eyert, G. Sangiovanni, G. Profeta, and V. N. Strocov, Phys. Rev. X **7**, 041067 (2017).